

GA-A27088

# TRANSPORT AND STABILITY OF HIGH- $\beta_N$ , HIGH NONINDUCTIVE FRACTION DIII-D DISCHARGES

by

F. TURCO, T.C. LUCE, J.R. FERRON, C.T. HOLCOMB,  
D.P. BRENNAN, J.C. DeBOO, A.E. WHITE,  
P.A. POLITZER and Y. IN

JULY 2011



## **DISCLAIMER**

**This report was prepared as an account of work sponsored by an agency of the United States Government. Neither the United States Government nor any agency thereof, nor any of their employees, makes any warranty, express or implied, or assumes any legal liability or responsibility for the accuracy, completeness, or usefulness of any information, apparatus, product, or process disclosed, or represents that its use would not infringe privately owned rights. Reference herein to any specific commercial product, process, or service by trade name, trademark, manufacturer, or otherwise, does not necessarily constitute or imply its endorsement, recommendation, or favoring by the United States Government or any agency thereof. The views and opinions of authors expressed herein do not necessarily state or reflect those of the United States Government or any agency thereof.**

# TRANSPORT AND STABILITY OF HIGH- $\beta_N$ , HIGH NONINDUCTIVE FRACTION DIII-D DISCHARGES

by

F. TURCO,<sup>1</sup> T.C. LUCE, J.R. FERRON, C.T. HOLCOMB,<sup>2</sup>  
D.P. BRENNAN,<sup>3</sup> J.C. DeBOO, A.E. WHITE,<sup>4</sup>  
P.A. POLITZER and Y. IN<sup>5</sup>

This is a preprint of a paper to be presented at the 38th European Physical Society Conference on Plasma Physics, Strasbourg, France on June 27 through July 1, 2011 and to be published in the Proceedings.

<sup>1</sup>Oak Ridge Associated Universities, Oak Ridge, TN USA

<sup>2</sup>Lawrence Livermore National Laboratory, Livermore, CA USA

<sup>3</sup>University of Tulsa, Tulsa, OK USA

<sup>4</sup>Massachusetts Institute of Technology, Cambridge, MA USA

<sup>5</sup>FAR-TECH, Inc., San Diego, CA USA

Work supported in part by  
the U.S. Department of Energy  
under DE-FC02-04ER54698, DE-AC52-07NA27344,  
DE-FC02-93ER54186 and DE-FG02-06ER84442

GENERAL ATOMICS ATOMICS PROJECT 30200  
JULY 2011

## INTRODUCTION

In order to create a scenario with high fusion gain and 100% noninductive current, a large fraction of the current must be sustained by bootstrap current ( $J_{BS}$ ). Under these conditions, the normalised ratio of plasma to magnetic pressure ( $\beta_N$ ) also has to be large, and the magnitude and location of  $J_{BS}$  are nonlinearly coupled with the evolution of the safety factor profile ( $q$ ), because of the feedback loop existing between  $q$ , transport and the kinetic profiles. Therefore, understanding the dependence of transport on the  $q$  profile in this regime is critical to the optimization. Moreover, high-performance, high noninductive current fraction plasmas are often limited by  $n=1$  tearing modes, that deteriorate the confinement and modify the current profile in a way that is not recoverable with the available current sources. For these reasons, experiments were conducted in the DIII-D tokamak, using systematic scans of  $q_{min}$  and  $q_{95}$ , at both fixed and maximum  $\beta_N$ , in order to determine empirically the variation of the transport properties with  $q$ , and the best alignment of the noninductive currents with the total current profile.

## ECCD INFLUENCES THE TEARING STABILITY

Electron cyclotron (EC) current is one of the sources used to provide part of the noninductive current required in excess of the bootstrap current. Experiments have shown that it has a positive influence on the tearing stability of the discharges, if aimed with a broad deposition at mid radius. Time traces from a model discharge are plotted in figure 1. The black traces show the stable discharge, while the red and the blue traces (with the same EC deposition location and profile) show that modes become unstable shortly after the EC power is turned off. The broad and relatively low power EC current profile differs substantially from the configuration used for direct stabilization of magnetic islands. Global current profile modifications are likely to be the mechanism at play, which influence directly the linear tearing index  $\Delta'$  of the equilibria. At fixed  $q_{min}$  and  $q_{95}$ , a broad EC deposition ( $\Delta\rho\sim 5-10$  cm) was injected at three different positions centred at  $\rho\sim 0.45, 0.55, 0.62$ . A

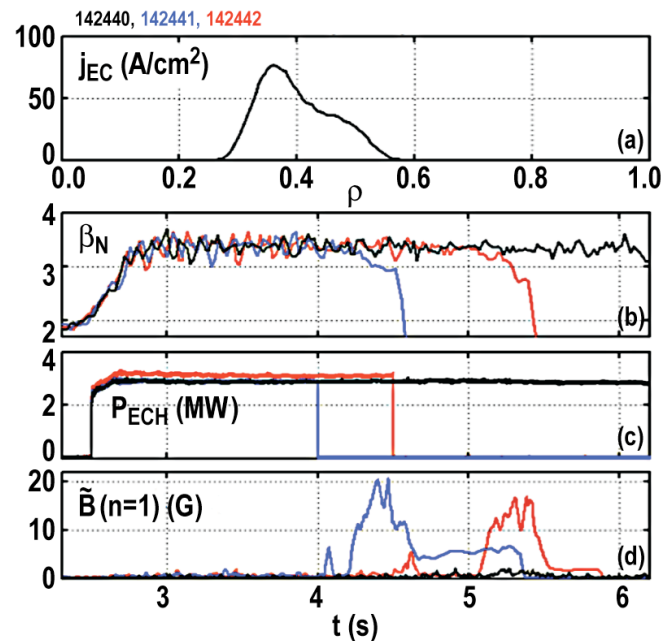


Fig. 1. Discharges from the ECCD deposition scans: (a) EC current profile, (b)  $\beta_N$ , (c) EC power, (d)  $n=1$  magnetic activity.

sample of the results of the EC scans are represented in figure 2, where it is shown that roughly 50% of the discharges with ECCD are stable, but tearing modes are still present in some cases (with both poloidal numbers  $m=2$  and  $m=3$ ). The variability of the outcome is consistent with the modeling results obtained with the PEST3 code. One of the experimental equilibria was analysed and the tearing and interchange indexes  $\Delta'$  and  $\Gamma'$  calculated. These show a sharp sudden increase when the plasma conditions approach the ideal MHD limit (figure 3), when an external kink instability is found by the model. When near the ideal limit (high  $\beta_N$ ), the plasma tearing stability becomes very sensitive to small changes in the equilibrium, as seen in the experiment.

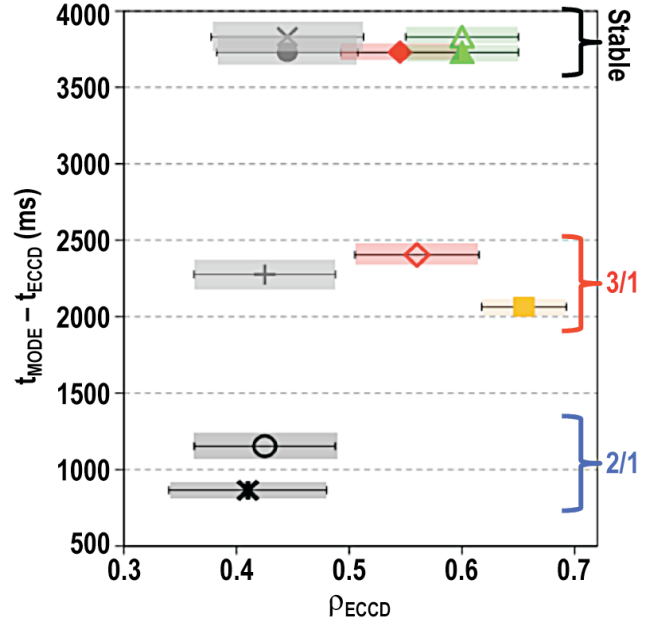


Fig. 2. Survival time of the ECCD scan discharges, against the deposition location and width. Stable discharges on the top of the plot, the type of  $n=1$  modes are indicated on the sides.

### THE $q$ PROFILE SCANS INDICATE THE PATH TO $f_{NI}=100\%$

The  $q$  profile scans were used to evaluate the NI current fraction and the  $J_{BS}$  magnitude and profile. Three values of  $q_{min}$  and  $q_{95}$  were used ( $q_{min} \sim 1.1, 1.5, 2$  and  $q_{95} \sim 4.5, 5.5, 6.8$ ) and the kinetic data were averaged over phases of both constant  $\beta_N \sim 2.8$  and maximum power. Ultimately, this allows evaluation of how transport affects the  $J_{BS}$  profile, which is a function of  $q$ ,  $\beta_N$  and the pressure peaking factor  $f_p$ . The sum of all the changes in the equilibria show that the kinetic profiles vary systematically and become broader for higher  $q_{min}$  and higher  $\beta_N$ . At constant  $\beta_N$ ,  $f_p$  decreases with increasing  $q_{min}$  (figure 4, blue circles), and it

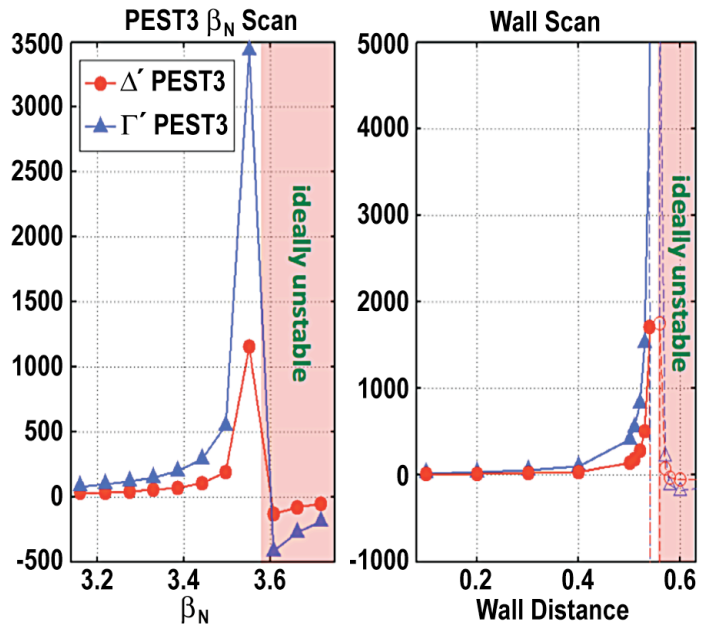


Fig. 3. PEST3  $\Delta'$  and  $\Gamma'$  indices, calculated for an experimental equilibrium. At fixed wall distance,  $\beta_N$  scan (left), at fixed pressure, wall distance scan (right).

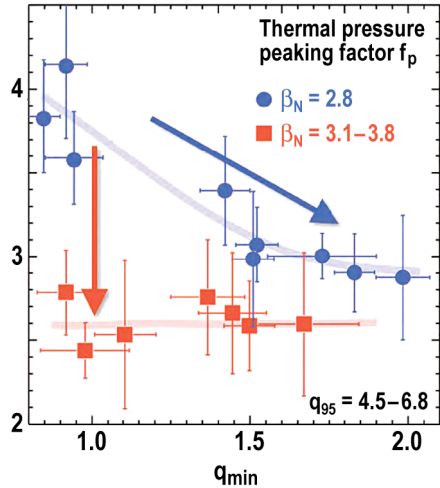


Fig. 4. Pressure peaking factor  $f_p$  for all the discharges, at fixed  $\beta_N=2.8$  (blue circles) and at maximum  $\beta_N$  (red squares), plotted against  $q_{\min}$  (all  $q_{95}$  values together).

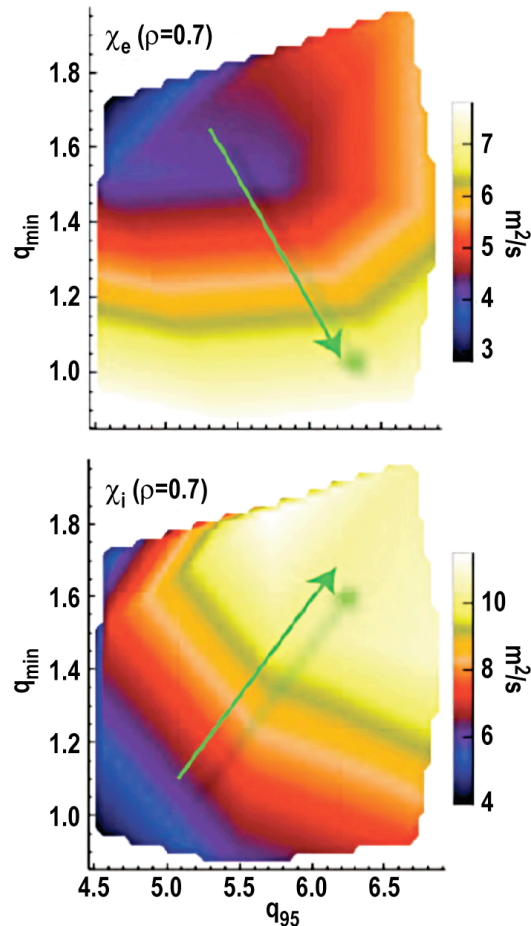


Fig. 5. Variations of  $\chi_e$  and  $\chi_i$  with  $q_{\min}$  and  $q_{95}$ , as evaluated from the experimental data.

decreases also for higher  $\beta_N$  values, becoming virtually insensitive to  $q_{\min}$  (red squares). The  $f_p$  trends, along with the changes in  $q$  and  $\beta_N$ , determine the  $J_{BS}$  profiles of the scan discharges:  $J_{BS}$  broadens with increasing  $q_{\min}$ , but most importantly at high  $\beta_N$  it loses the central peak and becomes roughly insensitive to  $q_{\min}$ . As a result, the bootstrap fraction increases with  $q_{95}$  and  $\beta_N$ , as expected, but it does not increase indefinitely with increasing  $q_{\min}$  [1].

## TRANSPORT EXPERIMENT AND MODELING

In order to investigate the reasons for the kinetic profiles variations described in the previous sections, heat transport coefficients ( $\chi_e$  and  $\chi_i$ ) were evaluated for all the discharges, and experimental density fluctuations were collected from the

Far InfraRed diagnostic. These data show that the electron and ion transport scales differently with  $q$  (figure 5):  $\chi_i$  increases with  $q_{\min}$  and  $q_{95}$ , while  $\chi_e$  decreases with  $q_{\min}$ . Electrons represent the dominant loss channel at low  $q_{\min}$ , while at high  $q_{\min}$  the ions dominate. The FIR data show the same trends with  $q$  for the energy available in the low wave numbers  $k_\theta$ , associated with ion mode activity, which therefore is consistent with the  $\chi_i$  trend. As a first step to evaluate models that could explain the results and guide the design of future experiments, the TGLF code was tested on the  $q$  scan discharges. Full radius runs were performed with and without the ExB shear and the experimental rotation profiles. The linear growth rates  $\gamma$  were also calculated at  $\rho=0.4, 0.5, 0.6, 0.7$ . The high wave number ( $k_\theta$ ) ranges vary with the  $q$  profile in a way that is not consistent with the experimental observations. Conversely, at low  $k_\theta$  the  $\gamma$  trend can explain the growth of  $\chi_i$  with  $q_{\min}$ , but it contradicts the transport variation with  $q_{95}$ . In the simulations, the gradients were allowed to relax and a sensitivity study was

performed to ensure that the results are not affected by systematic errors. Since the linear growth rates represent the energy available for the ion and electron transport in the plasma, these results suggest either that (i) the nonlinear saturation state must reverse the linear trends to make them follow the experimental observations, or that (ii) some physics is missing in the linear calculation [2].

## SUMMARY AND CONCLUSIONS

This study shows that the highest  $f_{NI}$  is reached at the highest  $q_{95}$  value, and the shape of the total  $J$  is best matched by  $J_{NI}$  at  $q_{min} \geq 1.5$  (figure 6). Since the bulk of the NI current is driven on axis by the neutral beam power, reaching higher  $\beta_N$  levels – positive for bootstrap current production – also entails the risk of overdriving the central current profile. The same can be said about the choice of higher  $q_{min}$  configurations. These conclusions, along with the need for additional off-axis current, motivated the installation of the new tilted neutral beam line, which is currently being used to explore higher  $q_{min}$  scenarios and different current alignments. The TGLF comparison with the experimental data indicates that the linear growth rate prediction of the code do not yet correlate with the measured transport rates, and more extensive (and possibly non-linear) work is needed to explain the physics mechanisms at play. The deposition location of  $J_{EC}$  that is attractive for tearing stability is also compatible with the position where the additional NI current is required. However, PEST3 results indicate that the approach to the ideal MHD limit makes the stability particularly sensitive to small changes in the equilibrium, and reproducibility of the results becomes an issue. For this reason, new modeling cases are being used to design equilibria with higher ideal and tearing limits.

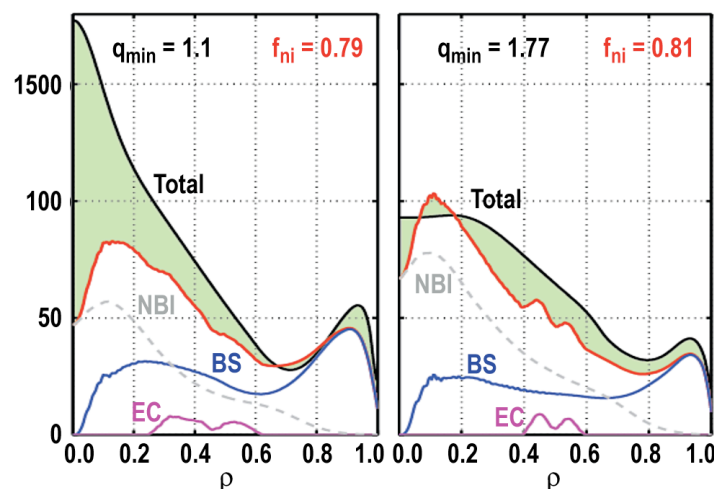


Fig. 6. Total  $J$  (black line) and alignment of the total NI current (red), neutral beam current (grey),  $J_{BS}$  (blue) and  $J_{EC}$  (purple) for the cases with lowest (left) and highest (right)  $q_{min}$ , at maximum  $\beta_N$ . The missing NI current is represented by the green shaded area.

## ACKNOWLEDGMENT

Work supported in part by the US Department of Energy under DE-FC02-04ER54698, DE-AC52-07NA27344, DE-FC02-93ER54186 and DE-FG02-06ER84442.

## REFERENCES

- [1] J.R. Ferron, Nucl. Fusion **51**, 063028 (2011).
- [2] C.T. Holcomb, “The effect of safety factor profile on transport in steady state, high performance scenarios,” submitted to Nucl. Fusion 2011.